CHEMISTRY
A EUROPEAN JOURNAL

DOI: 10.1002/chem.200500935

Nitrogen Fixation under Mild Ambient Conditions: Part I—The Initial Dissociation/Association Step at Molybdenum Triamidoamine Complexes

Boris Le Guennic,[a, b] Barbara Kirchner,[b] and Markus Reiher*[a]

Dedicated to Professor Dr. Siegfried Schneider on the occasion of his 65th birthday

Abstract: In several recent studies Schrock and collaborators demonstrated for the first time how molecular dinitrogen can be catalytically transformed under mild and ambient conditions to ammonia by a molybdenum triamidoamine complex. In this work, we investigate the geometrical and electronic structures involved in this process of dinitrogen activation with quantum chemical methods. Density functional theory (DFT) has been employed to calculate the coordination energies of ammonia and dinitrogen relevant for the dissociation/association step in which ammonia is substituted by dinitrogen. In the DFT calculations the triamidoamine chelate ligand has been modeled by a systematic hierarchy of increasingly complex substituents at the amide nitrogen atoms. The most complex ligand considered is an experimentally known ligand with an HMT = 3,5-(2,4,6-$Me_3C_6H_2)_2C_6H_3$ substituent. Several assumptions by Schrock and collaborators on key reaction steps are confirmed by our calculations. Additional information is provided on many species not yet observed experimentally. Particular attention is paid to the role of the charge of the complexes. The investigation demonstrates that dinitrogen coordination is enhanced for the negatively charged metal fragment, that is, coordination is more favorable for the anionic metal fragment than for the neutral species. Coordination of N_2 is least favorable for the cationic metal fragment. Furthermore, ammonia abstraction from the cationic complex is energetically unfavorable, while NH_3 abstraction is less difficult from the neutral and easily feasible from the anionic low-spin complex.

Keywords: density functional calculations · molybdenum · nitrogen fixation

Introduction

Catalytic dinitrogen reduction under mild ambient conditions at a structurally well-defined synthetic catalyst has been a Holy Grail in coordination chemistry.[1–4] A large number of dinitrogen complexes and potential intermediates have been synthesized—many of them inspired by the biological nitrogen reducing enzyme nitrogenase.[5–7] In 2003, Yandulov and Schrock[8,9] established the *first* abiological catalytic nitrogen fixation system based on a mononuclear molybdenum triamidoamine chelate complex [Mo($TerN_3N$)] (abbreviated as [Mo] in the following) with Ter = HIPT **1** (see Figure 1), which was a breakthrough in dinitrogen fixation research.[10,11] In a recent paper, Schrock and collaborators[12] examined Mo complexes **2**–**4** with three modified chelate ligands (with Ter = *p*BrHIPT, HMT, HTBT, respectively, in Figure 1).

Despite the comparatively small variations in the chelate ligands, remarkable consequences for the catalytic process have been observed. The authors state that "relatively subtle steric and electronic variations of the $[TerN_3N]^{3-}$ ligand system produce profound changes in the efficacy of the catalytic reduction of dinitrogen to ammonia"[12] and that "the catalytic reaction clearly is extremely finely balanced".[13] These changes in efficacy were then traced to key steps of the reduction cycle. It has been noted by Schrock and co-workers[12] that the reduction of the cationic ammine complex and exchange of ammonia by dinitrogen [Eq. (1)] are the steps most sensitive to a change in the $[TerN_3N]^{3-}$ chelate ligand.

[a] Dr. B. Le Guennic, Prof. Dr. M. Reiher
Institut für Physikalische Chemie
Universität Jena
Helmholtzweg 4, 07743 Jena (Germany)
Fax: (+49) 3641-948302
E-mail: markus.reiher@uni-jena.de

[b] Dr. B. Le Guennic, Dr. B. Kirchner
Lehrstuhl für Theoretische Chemie
Universität Bonn, Wegelerstrasse 12,
53115 Bonn (Germany)

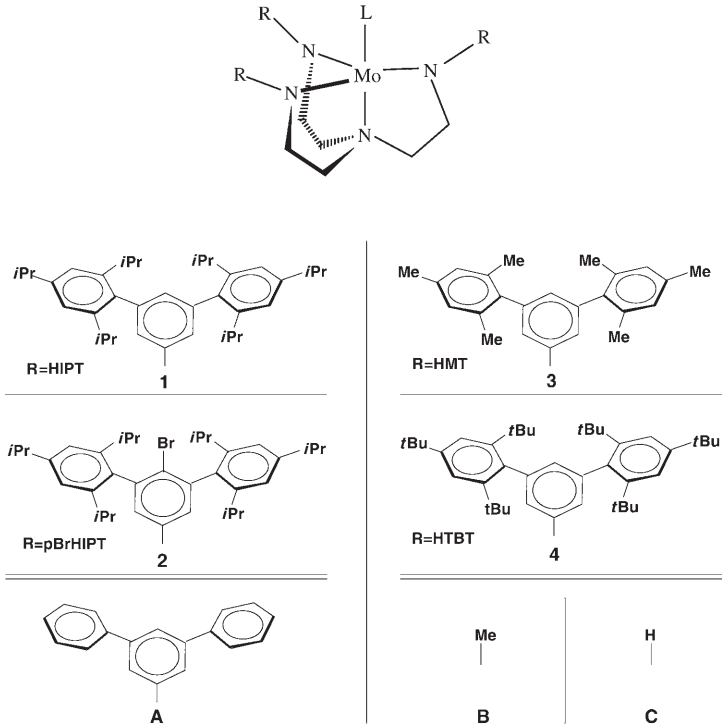

Figure 1. Structure of Schrock's dinitrogen reduction catalyst. The triamidoamine complex is experimentally known with four different ligands R = HIPT **1**, *p*BrHIPT **2**, HMT **3**, and HTBT **4** (HIPT = 3,5-(2,4,6-iPr$_3$C$_6$H$_2$)$_2$C$_6$H$_3$, *p*BrHIPT = 4-Br-3,5-(2,4,6-iPr$_3$C$_6$H$_2$)$_2$C$_6$H$_2$, HMT = 3,5-(2,4,6-Me$_3$C$_6$H$_2$)$_2$C$_6$H$_3$, HTBT = 3,5-(2,4,6-tBu$_3$C$_6$H$_2$)$_2$C$_6$H$_3$). For the computational investigations presented in this study we included three simplified models **A**, **B**, and for a methodological comparison of BP86 and B3LYP coordination energies the smallest model **C**.

$$[\mathrm{Mo}](\mathrm{NH_3})^{+} \xrightarrow{+e^-} [\mathrm{Mo}](\mathrm{NH_3}) \xrightarrow[-\mathrm{NH_3}]{+\mathrm{N_2}} [\mathrm{Mo}](\mathrm{N_2}) \qquad (1)$$

Hence, the first key step is the reduction of the cationic $[Mo](NH_3)^+$ to $[Mo](NH_3)$. Also sensitive are the equilibrium involving loss of ammonia to give the metal fragment [Mo] and the subsequent binding of dinitrogen. Yandulov and Schrock[13] stress that "Although replacement of ammonia by dinitrogen in dinitrogen reduction schemes has been postulated for decades, upon reflection it is difficult to imagine two η^1 ligands that are more different in how they bind to the same site in a Mo^{III} complex. The mechanism, equilibrium, and rate of conversion of $[Mo](NH_3)$ to $[Mo](N_2)$ therefore are of great importance."

The aim of this quantum chemical study is to shed light on these key reactions and to provide insight into the role of the chelate ligand. For this purpose it is mandatory to include the experimentally known ligands as well as simplified models. From experiment we chose the "small" system **3** with the HMT substituent at the amide nitrogen atoms (see Figure 1) although less experimental data are available for complex **3** relative to complex **1**. The lack of experimental data on **3** is due to solubility reasons,[12] but experiments with different solvents also indicate that the catalytic activity of **3** is reduced compared to the original derivative **1**. However, the complexes **1**, **2**, and **4** require significantly larger computational times relative to **3**, because of the increased number of stable conformers due to the larger alkyl substituents *i*Pr and *t*Bu. A comparison of complexes **1** to **4** is thus beyond the scope of this work and will be presented in a future study.

Due to the size of the triamidoamine complexes only quantum chemical methods based on density functional theory (DFT) are feasible. Here, we will also assess the reliability of different density functionals for Schrock's complexes, which may also be important for the assessment of DFT studies on the biological active site, that is, the FeMo cofactor (FeMoco) of nitrogenase. All theoretical studies of FeMoco lack a direct comparison with experiment. For example, the structure of FeMoco is only known for the resting state and not even the charge of the FeMoco cluster or the spin state during reduction are known with certainty. Nonetheless, sophisticated DFT studies on the FeMoco of nitrogenase have been carried out.[14–22] Though these calculations were performed at very high standards, a final answer on the mechanism of nitrogenase has not yet been found, as they do not agree in essential parts of the mechanism. For example, in reference [14] N_2 adsorption at the "surface" of the FeMoco is postulated, while FeMoco opening according to Sellmann's open-side model[3] is found in reference [15]. Furthermore, the mechanisms postulated in references [14] and [15] exclude an exchange of the central nitrogen atom, while it is exchanged in the hypothetical mechanism given in reference [19]. Also, the molybdenum atom was excluded as the coordination site of dinitrogen. This exclusion was made on the basis of electronic energy differences of minimum structures, which turned out to be as small as 26 kJ mol^{-1} in isolated FeMoco model systems.[19] In reference [22] molybdenum is considered as the N_2 coordinating center. Furthermore, all DFT studies on FeMoco rely on pure density functionals like (R)PBE[23,24] and BP86,[25,26] while it is well known that the energetical ordering of different spin states can hardly be reproduced without inclusion of exact exchange in critical cases.[27–36] Very recently Graham et al.[37] presented a sophisticated comparison of DFT and coupled cluster results for nitrogen activation at a three-coordinate molybdenum metal fragment yielding tetrahedral dinuclear dinitrogen complexes. They found B3LYP energies in agreement with CCSD(T) results, while other density functionals yield substantially different results. For this reason, we rely on the pure functional BP86 and the hybrid functional B3LYP in this work in order to arrive at functional-independent and consistent results. Note that Graham et al. found our B3LYP* functional[27,29,30] to yield the same results as B3LYP. Since much more experience has been gained with B3LYP, we also stick to the B3LYP functional instead of B3LYP* in this work.

The role of Mo is evident in Schrock's complex and has often been considered essential for dinitrogen binding by various authors (see also the recent work in references [38–44]). Very recently, studies on molybdenum complexes have been reported,[45,46] which discuss results for intermediate steps of N_2 reduction in the light of Yandulov and Schrock's

remarkable catalytic system. Although the iron atoms in FeMoco may play the decisive role in biological nitrogen reduction, our focus here will be on the central molybdenum atom in Schrock's complex, because of the wealth of detailed experimental data available on this well-defined system.

The present investigation aims at two major goals. First, the quantum chemical calculations shall provide a detailed insight into the key steps of Schrock's mechanism and then help to clarify the role of the ligand. Second, our study shall provide an assessment of the confidence interval of DFT studies on nitrogen fixation.

Computational Methods

For all calculations we employed the density functional programs provided by the TURBOMOLE 5.1 and 5.6 suites.[47] Results were obtained from Kohn–Sham optimizations of all investigated structures. We used the Becke–Perdew functional dubbed BP86[25,26] and the hybrid functional B3LYP[48,49] as implemented in TURBOMOLE. For all closed-shell electronic structures we employed a restricted framework, while we switched to unrestricted Kohn–Sham calculations for the open-shell complexes. In connection with the BP86 functional we applied the resolution-of-the-identity (RI) density-fitting technique with auxiliary bases by Eichkorn et al.[50,51] in order to speed up the calculations. For the experimentally known complex **3** we employed Ahlrichs' TZVP basis set,[52] featuring a valence triple-zeta basis with polarization functions on the molybdenum and nitrogen atoms, while the carbon and hydrogen atoms carried the smaller split valence plus polarization functions SVP basis set.[53] All small models **A**, **B**, and **C** (depicted in Figure 1) were optimized within the TZVP basis set for all atoms. For the molybdenum atom an effective core potential (ECP) from the Stuttgart group was applied.[54] This ECP also guarantees a reliable description of scalar-relativistic effects on molybdenum. Population analyses were performed within the Davidson–Roby–Ahlrichs scheme[55,56,57] as implemented in TURBOMOLE.

All BP86 and B3LYP data are reported for fully optimized structures. These two functionals were chosen since they are the most well-established representatives of pure and hybrid density functionals yielding reasonable reaction energetics and molecular structures in a large number of cases.[58] Especially, the BP86 functional is well established for the calculation of reliable structural parameters of transition-metal complexes (compare, for example, references [58,27,59–61]). However, in cases in which states of different spin need to be considered, the situation turned out to be different and unreliable energetics have been obtained for transition-metal complexes; see, for instance, references [27,59] and the recent review by Harvey.[62]

To analyze the electronic structure of the molybdenum–triamidoamine complexes within an occupation-number-independent picture, calculations based on extended Hückel theory (EHT)[63] were carried out on the BP86-optimized structures of the small model complexes [Mo](N_2) and [Mo](NH_3) of series **B** (see Figure 1) by using the CACAO program.[64] The Slater exponents (ζ) and the valence-shell ionization potentials (H_{ii} in eV), respectively, were set to: 1.3, −13.6 for H 1s; 1.625, −21.4 for C 2s; 1.625, −11.4 for C 2p; 1.950, −26.0 for N 2s; 1.950, −13.4 for N 2p; 1.960, −8.34 for Mo 5s; 1.900, −5.24 for Mo 5p. The H_{ii} value for Mo 4d was set equal to −10.50 eV. A linear combination of two Slater-type orbitals with exponents $\zeta_1 = 4.54$ and $\zeta_2 = 1.90$ and with the weighting coefficients $c_1 = 0.5899$ and $c_2 = 0.5899$ was employed to represent the Mo 4d atomic orbitals. It should be emphasized that the EHT calculations do not account for spin-orbit splittings of the one-electron p and d states and thus include at most spin-averaged scalar relativistic effects.

Complex **3** exhibits a huge number of local minima on the potential-energy hypersurface connected through rotations of the methyl and phenyl substituents. Since such a magnitude of conformers cannot appropriately be examined by means of static quantum chemical calculations, we started all structure optimizations from the same initial structure of the chelate ligand in order to avoid artificial energy differences stemming from conformational energy differences in the chelate ligand. Furthermore, we initially tested that internal rotation of the phenyl rings does not lead to more stable conformers. (All optimized Cartesian coordinates may be obtained from the authors.)

Results and Discussion

Models and optimized structures: To systematically study the steric and electronic effects of the chelate ligand, we started with the smallest possible model for a triamidoamine ligand, namely with model complex **C** [Mo{$(HNCH_2CH_2)_3N$}]. However, structure optimization for this model with NH_3 as fifth ligand led to pyramidalized amide nitrogen atoms when using the B3LYP density functional. That is, two out of three amide nitrogen atoms showed a pyramidalized structure in contradiction with experiment. For this reason, the smallest model **C** serves only for a methodological comparison of BP86 and B3LYP coordination energies. We should note that after submission of this paper a DFT study by Studt and Tuczek on the full catalytic cycle as proposed by Schrock and collaborators was published,[65] which was solely based on the small model **C**. These authors did not observe the pyramidalization in the B3LYP calculations, but employed different basis sets and effective core potentials in the structure optimization.

In model **B** [Mo{$(MeNCH_2CH_2)_3N$}], in which the hydrogen atoms at the amide nitrogen atoms of **C** have been substituted by methyl groups, no pyramidalized amide nitrogen atoms show up after structure optimizations. The next largest model **A** [Mo{$(LNCH_2CH_2)_3N$}] with L = 3,5-$(C_6H_5)_2C_6H_3$ features the generic chelate ligand, which closely resembles the experimentally known system without substituents at the phenyl rings. Finally, we include in our study the smallest of the experimentally known complexes, system **3** [Mo{$(HMTNCH_2CH_2)_3N$}] with HMT = 3,5-(2,4,6-$Me_3C_6H_2)_2C_6H_3$. The BP86/RI-optimized structures of the two models **A** and **B** as well as of system **3** are depicted in Figure 2 with N_2 as the fifth ligand.

Table 1 contains selected structural parameters of the optimized complexes relevant for the study of the initial NH_3 dissociation and N_2 association step(s). Since some complexes have also been optimized with the B3LYP density functional in order to test the calculated energetics for internal consistency, it is also worth to compare the structures obtained for both functionals. First of all, we note that the Mo–N_{ad} bond lengths optimized with BP86/RI and B3LYP are in excellent agreement; the differences are within 0.01 Å. This is also the case for most of the other bond lengths. Even the relevant bond angles are in excellent agreement. Only few bond lengths in Table 1 deviate by more than 0.01 Å. Examples are found for the Mo–N_α distance and for the triple bond in the dinitrogen ligand. In the latter case, the B3LYP N≡N bond length is closer to the ex-

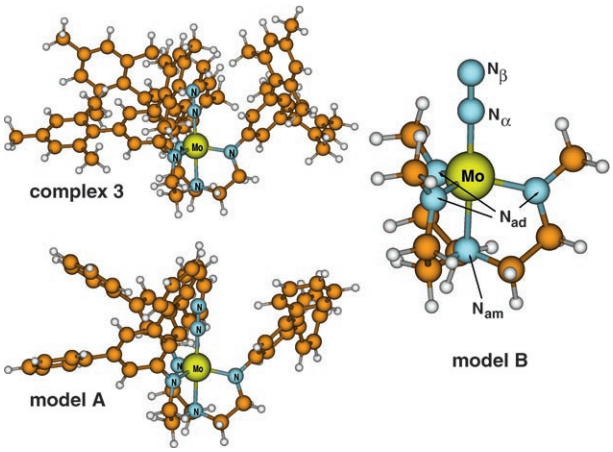

Figure 2. BP86-optimized structures of [Mo](N_2) for system **3**, model **A**, and model **B**.

perimental value of 1.0977 Å,[66] while the BP86/RI value deviates by about 0.04 Å. However, when it comes to the calculation of metal–ligand bond lengths the reverse situation often appears to be the case and the BP86 metal–ligand distances are in better agreement with experiment than the B3LYP distances are (see also the references given in the Computational Methods section). Nonetheless, for the molybdenum–nitrogen bonds, the deviations are usually less than about 0.02 Å, which is very satisfactory—especially as we need to compare with the experimental value for a different ligand, namely, for complex **1** (see Table 2), because experimental bond lengths are not yet available for complex **3**. In view of the good agreement of the structural parameters calculated with the two different density functionals and for the sake of brevity, we restrict the following discussion to BP86/RI structural parameters.

Comparing the calculated structural parameters for the three systems **3**, **A**, and **B** we note that the overall structures are similar. Depending on the chelate ligand, bond length variations of about 0.02 Å can be observed. The most interesting structural parameter is the N≡N bond length (column 5 in Tables 1 and 2): it is almost equal for all neutral (1.142–1.148 Å), all cationic (1.128–1.130 Å), and all anionic complexes (1.163–1.170 Å). Hence, reduction of the neutral complexes results in an elongation of the triple bond by 0.02 Å. Model **B** shows the largest bond elongation by 0.042 Å of the cationic species upon double-electron transfer to yield the anionic species.

The bond lengths of Mo to the amide nitrogen atoms (column 2 in Tables 1 and 2) as well as to the *trans*-amine nitrogen atom (column 3 in Tables 1 and 2) in the neutral and cationic species show systematic trends from complex **B** to **A** to **3**, which can be assigned to the increased strain induced by the bulkier ligands. In fact, the chelate ligand in complex **3** exhibits pronounced steric demands and provides only a rather small cavity for the reduction reactions to take place. However, the trends are less evident in the anionic complexes.

Interestingly, the negatively charged [Mo]$(N_2)^-$ species possess linear Mo–N≡N moieties with an elongated N≡N bond length. Thus, the triple bond remains essentially intact in the anionic complexes, which is in agreement with what is experimentally known for complex **1**. An alternative reaction of the N_2 ligand could have been the formation of a double bond,

Table 1. Selected structural parameters of the three molybdenum triamidoamine complexes (BP86/RI/TZVP-SVP for complex **3**; BP86/RI/TZVP for models **A** and **B**; for some structures we also obtained B3LYP-optimized structures for internal consistency checks, which are given in brackets) [distances and angles are given in Å and degrees, respectively; notation is according to Figure 2]. A comparison with the X-ray structural data available for the original complex **1** is given in Table 2.

	Mo–N_{ad}[a]	Mo–N_{am}[b]	Mo–N_α	N_α–N_β	N_{am}-Mo-N_α	Mo-N_α-N_β
complex **3**						
[Mo]$^-$	2.033	2.146				
[Mo]	2.012	2.149				
[Mo]$^+$	1.971	2.201				
[Mo](N_2)$^-$	2.041	2.259	1.925	1.163	178.9	179.4
[Mo](N_2)	2.011	2.245	1.982	1.143	178.3	178.3
[Mo](N_2)$^+$	1.980	2.268	2.045	1.130	175.0	174.9
[Mo](NH_3)$^-$	2.027	2.214	2.284		177.8	
[Mo](NH_3)	2.020	2.208	2.284		176.7	
[Mo](NH_3)$^+$	1.979	2.252	2.278		174.1	
model **A**						
[Mo]$^-$	2.025	2.136				
[Mo]	2.008	2.138				
[Mo]$^+$	1.967	2.202				
[Mo](N_2)$^-$	2.049	2.262	1.922	1.164	178.5	179.4
[Mo](N_2)	2.009	2.236	1.991	1.142	177.4	178.2
[Mo](N_2)$^+$	1.974	2.264	2.058	1.129	175.7	175.4
[Mo](NH_3)$^-$	2.024	2.202	2.316		176.4	
[Mo](NH_3)	2.016	2.205	2.293		175.0	
[Mo](NH_3)$^+$	1.976	2.262	2.272		164.0	
model **B**						
[Mo]$^-$	2.031 [2.053]	2.116 [2.165]				
[Mo]	2.000 [2.008]	2.128 [2.149]				
[Mo]$^+$	1.944 [1.943]	2.187 [2.199]				
[Mo](N_2)$^-$	2.031 [2.042]	2.241 [2.261]	1.922 [1.935]	1.170 [1.148]	179.8 [179.8]	179.7 [179.8]
[Mo](N_2)	2.002 [2.005]	2.229 [2.228]	1.978 [2.013]	1.148 [1.125]	178.5 [178.4]	178.7 [178.4]
[Mo](N_2)$^+$	1.954 [1.950]	2.261 [2.260]	2.066 [2.125]	1.128 [1.107]	177.6 [177.6]	178.2 [178.0]
[Mo](NH_3)$^-$	2.041 [2.067]	2.170 [2.204]	2.357 [2.409]		173.9 [177.2]	
[Mo](NH_3)	2.016 [2.023]	2.179 [2.198]	2.329 [2.351]		179.0 [179.0]	
[Mo](NH_3)$^+$	1.957 [1.957]	2.257 [2.265]	2.316 [2.327]		173.1 [174.7]	

[a] Averaged Mo–N(amide) distance. [b] Mo–N(amine) distance.

Table 2. Comparison between calculated (complex **3** and models **A** and **B**) and experimental (complex **1**; reference [8]) bond lengths; the latter are given in bold face [distances are given in Å; notation is according to Figure 2].

	$Mo–N_{ad}$[a]	$Mo–N_{am}$[b]	$Mo–N_{\alpha}$	$N_{\alpha}–N_{\beta}$
$[Mo](N_2)$				
3	2.011	2.245	1.982	1.143
A	2.009	2.236	1.991	1.142
B	2.002	2.229	1.978	1.148
1	**1.978**	**2.188**	**1.963**	**1.061**
$[Mo](N_2)^-$				
3	2.041	2.259	1.925	1.163
A	2.049	2.262	1.922	1.164
B	2.031	2.241	1.922	1.170
1	**2.030**	**2.241**	**1.863**	**1.156**
$[Mo](NH_3)$				
3	2.020	2.208	2.284	
A	2.016	2.205	2.293	
B	2.016	2.179	2.329	
1	**2.003**	**2.205**	**2.170**	
$[Mo](NH_3)^+$				
3	1.979	2.252	2.278	
A	1.976	2.262	2.272	
B	1.957	2.257	2.316	
1	**1.948**	**2.147**	**2.236**	

[a] Averaged Mo–N(amide) distance. [b] Mo–N(amine) distance.

which, for instance, has been observed as a viable N_2-bond activation process in quantum chemical studies on iron(II)–sulfur complexes.[67,68] The fact that this alternative activation mechanism, which would exhibit a characteristic bending of the Mo-N-N unit from 180° to up to 120° owing to the emerging nitrogen lone-pairs, is not observed indicates that the excess charge of the anionic complex does not populate the antibonding π orbital of the N_2 ligand in significant amounts. Rather it is located on the molybdenum central ion, which then increases the amount of back-bonding resulting in an elongation of the triple bond (see also the population analyses discussed below).

Except for one bond length (namely, $Mo–N_{am}$ in the ammine model **B**, $[Mo](NH_3)$), all calculated distances are found equal or slightly larger than the experimental bond lengths in complex **1**. However, a few calculated distances are more than 0.1 Å larger than the experimental ones. This is, for instance, the case for the $Mo–N_{am}$ and $Mo–N_{\alpha}$ distances in $[Mo](NH_3)^+$ and $[Mo](NH_3)$, respectively. These differences are likely due to the fact that we are comparing different chelate ligand derivatives.

Interestingly, Schrock et al.[13] observed for the reduction of $[Mo](NH_3)^+$: "One-electron reduction of $[Mo](NH_3)^+$ leads to a slight lengthening of $Mo–N_{amide}$ distances (by an average of 0.05 Å), shortening of the $Mo\leftarrow NH_3$ bond (by 0.07 Å), and lengthening of the trans $Mo\text{-}N_{amine}$ bond (by 0.06 Å). While these small changes in bond distances in general are consistent with an electron being added to a d_{xz} or d_{yz} orbital on Mo, why the $Mo\leftarrow NH_3$ bond shortens upon reduction of $[Mo](NH_3)^+$ to $[Mo](NH_3)$ is not clear to us". While we can confirm the bond elongations of $Mo–N_{amide}$ and $Mo–N_{amine}$ for systems **3**, **A**, and **B**, we do not observe a bond contraction of the $Mo\leftarrow NH_3$ ligand bond. By contrast, this coordinative bond is elongated in all model complexes investigated here. We observe a lengthening of the calculated $Mo\leftarrow NH_3$ bond (by 0.006, 0.021, and 0.013 Å for complex **3**, model **A**, and model **B**, respectively) and a shortening of the calculated $Mo–N_{amine}$ bond (by 0.044, 0.057, and 0.078 Å for complex **3**, model **A**, and model **B**, respectively). The reason for the experimentally observed contraction of this bond in complex **1** thus remains unclear and cannot be explained on the basis of the calculations. Either the different structure of the chelate ligand of complex **1** when compared with the systems **3**, **A**, or **B** or a crystal packing effect are responsible for this contradiction. The latter is more likely in view of the same trends observed for our three different systems **3**, **A**, and **B** as opposed to the experimentally investigated complex **1**. It appears to be unlikely that the local electronic structure at the central molybdenum ion is responsible for the experimentally observed bond contraction.

Qualitative picture of the electronic structure: For a qualitative understanding of the electronic structure of a transition-metal complex, occupation-number-independent EHT calculations represent a very valuable tool. Hence, we carried out such calculations for the BP86-optimized structures of the N_2 and NH_3 complexes. We selected the small model complex **B** in order to keep the spectrum of orbital energies as sparse as possible. This selection is justified in view of the similar structural parameters of the three complexes under consideration. The electronic structure of model complex **B** with dinitrogen as fifth ligand is depicted in Figure 3. This figure contains the correlation diagram for the interaction of the frontier orbitals of the triamidoamine–metal fragment with those of dinitrogen. The occupation chosen is for the open-shell neutral doublet complex.

While the occupied π-orbitals 3a and 4a of the dinitrogen ligand do not participate in the metal–N_2 interaction, the rotationally symmetric bonding orbital 5a of N_2 experiences a significant stabilization upon interaction with the Mo d_z orbital. Also, the EHT molecular orbital diagram clearly shows a stabilization of the N_2 coordination by an interaction of the frontier d orbitals at molybdenum with the antibonding π_g orbitals of dinitrogen, resulting in a decrease in orbital energy and transfer of charge into the antibonding orbitals by means of a back-donation mechanism.

From the qualitative MO diagram in Figure 3 we may anticipate that the electron affinity (EA) is likely to be exothermic or slightly endothermic, since an energy-lowered frontier orbital localized at the molybdenum–N_2 moiety will be occupied to yield a stable closed-shell singlet structure. This stabilization of the system is indeed accompanied by a contraction of the $Mo–N_{\alpha}$ bond as documented in Table 1 for all systems. With regard to the first ionization energy of the dinitrogen-coordinated model **B** we note that an electron would have to be removed from the same stabilized

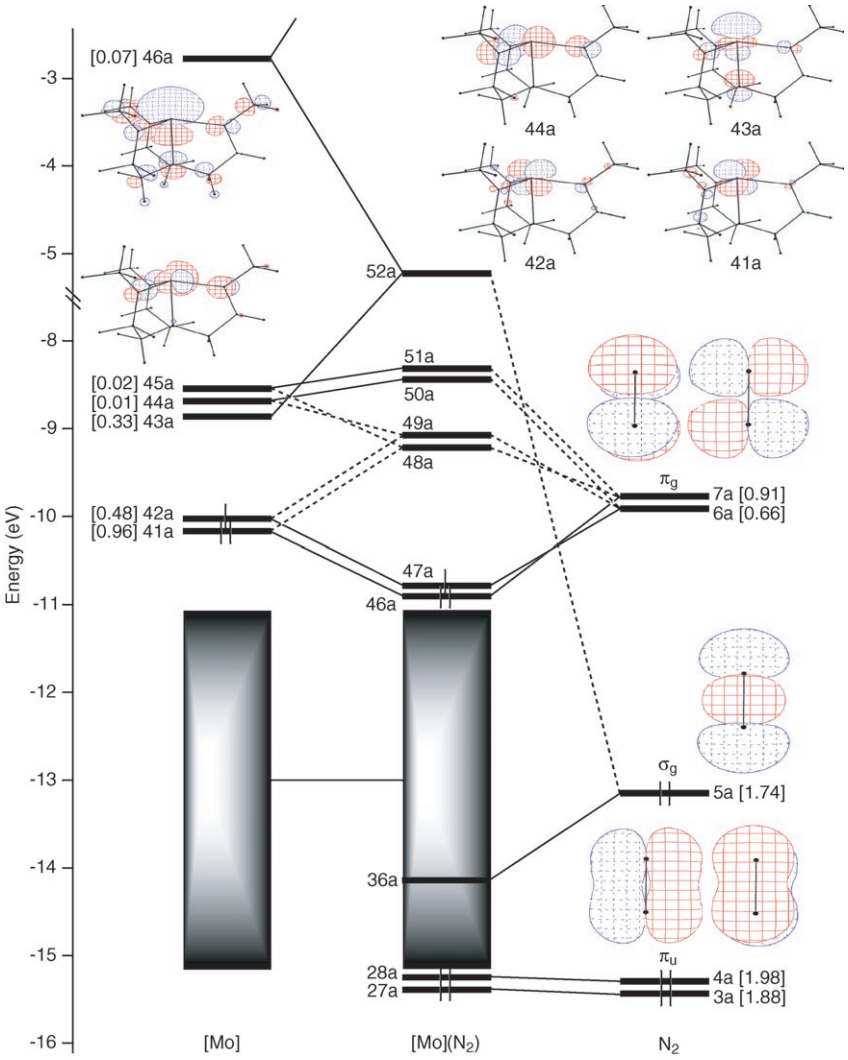

Figure 3. EHT orbital interaction diagram for the model complex **B** [Mo](N_2). Fragment molecular orbital occupancies after interaction are given in brackets. The formal occupation depicted corresponds to the neutral system. The extended dark boxes mark dense lying molecular orbitals of the metal fragment that do not contribute to a qualitative understanding of N_2 coordination.

frontier molecular orbital (47a). This would result in an increased amount of energy required for ionization. Accordingly, the Mo–N_α bond length is expected to increase and the Mo–N_{ad} bond lengths to shorten with decreasing molecular charge (see Table 1).

Figure 4 depicts the EHT frontier molecular orbital interaction diagram for the ammine complex of model **B**. Coordination of NH_3 is facilitated by the σ-donating orbital 4a interacting with the molybdenum d orbital of proper local symmetry. However, the resulting decrease in energy is smaller than in case of N_2 coordination, indicating that the coordination energies might be of comparable strengths tunable through the charge state of the complex. In contrast to the N_2 complex, the ammine system **B** cannot benefit from a back-donation mechanism owing to the lack of π orbitals; the [Mo] d-frontier orbitals 41a and 42a remain nonbonding (see Figure 4). From the highest occupied frontier orbital of the MO diagram in Figure 4, we understand that the electron affinity of the ammine complex should be less "exothermic" when compared with the dinitrogen system, while the ionization energy should be less "endothermic".

Experimentally it is known for complex **1** (reference [13]) that "the $[Mo](N_2)^{+/0}$ potential is almost 1 V higher than the value for $[Mo](NH_3)^{+/0}$ (−0.66 V vs −1.63 V), that is, $[Mo](NH_3)^+$ is more difficult to reduce than $[Mo](N_2)^+$ by ~1 V". This substantial difference has been ascribed to the stronger σ-donating properties of ammonia as well as to the fact that the electron added to $[Mo](N_2)^+$ can occupy a π-bonding orbital. The EHT orbital interaction diagrams of $[Mo](N_2)$ and $[Mo](NH_3)$ in Figures 3 and 4 thus confirm these assumptions. However, the slightly stronger σ donation of NH_3 compared to N_2 is only evident from the occupancies of the fragment orbitals after interaction, which are 1.72 and 1.74 for the 4a (N_2) and 5a (NH_3) σ-type fragment molecular orbitals, respectively. It is not substantiated from an energetical point of view as described above. Also, whereas the LUMO (46a) of $[Mo](NH_3)^+$ is almost exclusively of d_{xz} type (or d_{yz}) on Mo, the first unoccupied orbital of $[Mo](N_2)^+$ (47a) correrspondes to the bonding interaction of the same d_{xz}-type orbitals with π-type orbitals of the dinitrogen fragment. This orbital is thus stabilized and can facilitate the addition of an electron. This stabilization of the LUMO when replacing the NH_3 group by a N_2 fragment is visible in the self-consistent DFT calculations for neutral and cationic complexes of NH_3 and N_2 studied (see Table 3). The effect is also visible, but much less pronounced for the anionic complexes, which are therefore not included in Table 3.

Ionization energies and electron affinities: For the exchange of ammonia and dinitrogen in catalytic dinitrogen reduction it is important to understand, in which order the reduction and exchange steps are carried out. Therefore, we first investigate oxidation and reduction reactions with correspond-

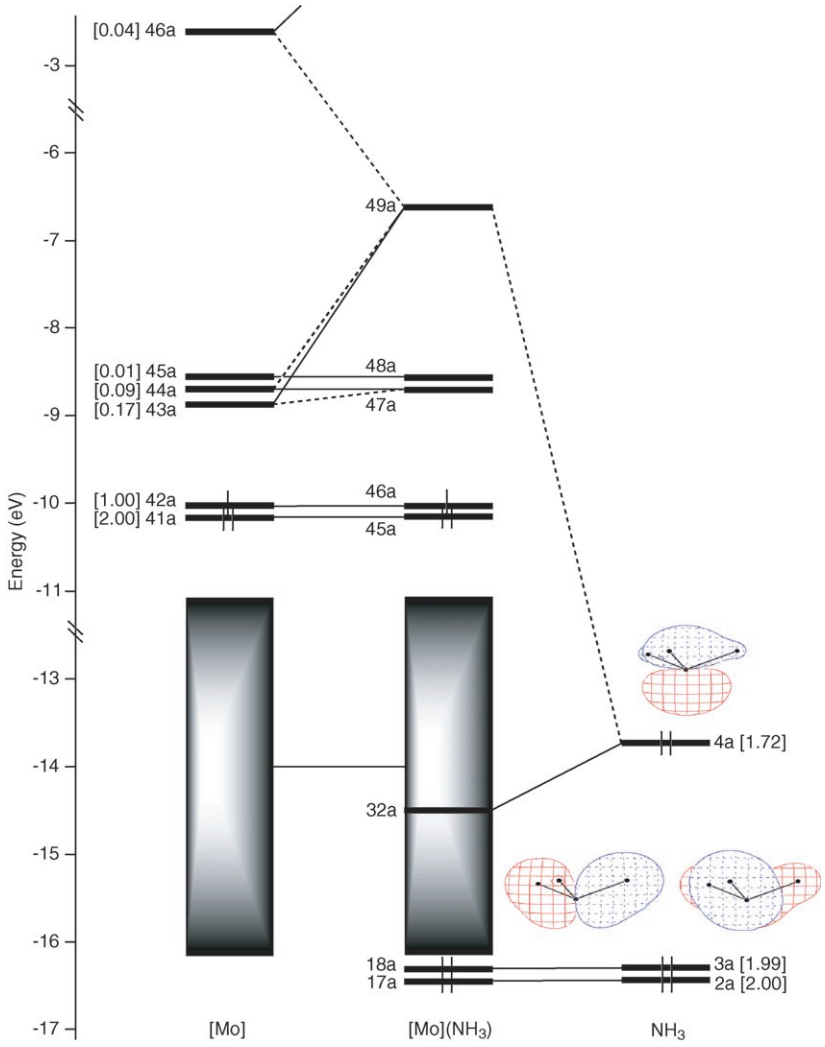

Figure 4. EHT orbital interaction diagram for the model complex **B** [Mo](NH_3). Fragment molecular orbital occupancies after interaction are given in brackets. The formal occupation depicted corresponds to the neutral system. See Figure 3 for plots of the main molecular orbitals of the [Mo] fragment of complex **B**.

Table 3. Calculated BP86 HOMO and LUMO energies [in eV] for [Mo](NH_3)$^+$ and [Mo](N_2)$^+$ of system **3** and models **A** and **B** (basis sets as described above). Replacing NH_3 by N_2 yields a consistent lowering of the orbital energies independent of the charge. For model **B** we have also included the orbital energies obtained from the B3LYP optimizations.

		complex **3** BP86/RI	model **A** BP86/RI	model **B** BP86/RI/B3LYP
[Mo](NH_3)$^+$	HOMO	−5.94	−6.14	−6.65/−7.81
	LUMO	−5.91	−5.86	−5.92/−5.17
[Mo](N_2)$^+$	HOMO	−7.01	−7.17	−7.98/−8.81
	LUMO	−6.66	−6.68	−7.20/−6.38
[Mo](NH_3)	$HOMO_\alpha$ = HOMO − 1	−2.76	−2.89	−2.09/−3.02
	$HOMO_\beta$ = HOMO	−2.42	−2.55	−1.73/−2.64
	$LUMO_\beta$ = LUMO	−2.11	−2.24	−1.40/−0.32
	$LUMO_\alpha$ = LUMO + 1	−1.39	−1.96	−0.63/−0.13
[Mo](N_2)	$HOMO_\alpha$ = HOMO − 1	−3.98	−4.04	−3.69/−4.44
	$HOMO_\beta$ = HOMO	−3.73	−3.79	−3.43/−4.12
	$LUMO_\beta$ = LUMO	−3.38	−3.45	−3.13/−2.14
	$LUMO_\alpha$ = LUMO + 1	−1.65	−1.93	−1.11/−0.31

ing ionization energies IE_i and electron affinities EA_i. Before we discuss the results, we should have a look on the BP86/RI versus the B3LYP ionization energies and electron affinities. For comparison, we collected some data in Table 4.

Large discrepancies between the BP86/RI and the B3LYP energies for the **C** series of model complexes are caused by a pronounced structural distortion of the metal fragment in the ammine complex. This distortion manifests in a pyramidalization of two out of the three amide nitrogen atoms (see also Sect. 3). When B3LYP single point calculations are carried out for the ammine complex of **C** on the BP86/RI optimized structures, the discrepancies between B3LYP and BP86/RI energies are diminished as can be understood from Table 4.

The electron affinity of the [Mo](N_2)$^+$ complexes in Table 4 (fourth line in upper block) is not affected by the choice of the functional and we obtain almost the same results for BP86/RI and B3LYP. The corresponding calculation for the [Mo](NH_3)$^+$ complex of model **B** shows a small difference between BP86/RI and B3LYP of −12.12 kJ mol^{-1}. When we look at the electron affinities we note deviations of BP86/RI from B3LYP between 22.86 and 29.44 kJ mol^{-1}, which are small in view of the general accuracy of DFT calculations. Based upon this comparison of density functionals we may conclude that it is justified to restrict the discussion of energies to the BP86/RI data only. The calculated adiabatic energies for these electron-transfer reactions have been obtained from fully optimized species and are given in a combined map of reaction pathways depicted in Figure 5.

Table 4. Comparison of reaction energies for model complexes **C** and **B** [in kJ mol^{-1}]. In cases of large discrepancies, the B3LYP energies have been marked in bold face. The common element in all these reactions is the ammine complex of model **C**, which turned out to be structurally distorted at one amide nitrogen atom. A B3LYP single-point calculation for this [Mo](NH$_3$) complex of series **C** on its BP86/RI/TZVP-optimized structure recovers the general trends of BP86 and B3LYP results (results are given in parenthesis). Δ denotes the energy difference.

			model **C**			model **B**		
reactants		products	BP86/RI	B3LYP	Δ	BP86/RI	B3LYP	Δ
reduction processes								
$[Mo](NH_3)^+ + e^-$	→	$[Mo](NH_3)$	−435.18	**−359.56** (−442.01)	**+75.62** (−6.83)	−427.79	−439.91	−12.12
$[Mo](NH_3) + e^-$	→	$[Mo](NH_3)^-$	+63.29	**+18.02** (+100.47)	**−45.27** (+37.18)	+60.06	+89.50	+29.44
$[Mo](N_2) + e^-$	→	$[Mo](N_2)^-$	−79.66	−55.82	+23.84	−96.43	−73.57	+22.86
$[Mo](N_2)^+ + e^-$	→	$[Mo](N_2)$	−564.93	−562.18	+2.75	−540.00	−540.63	−0.63
ligand exchange processes								
$[Mo](NH_3)^+ + N_2$	→	$[Mo](N_2)^+ + NH_3$	+41.76	+70.27	+28.51	+25.43	+56.94	+31.51
$[Mo](NH_3) + N_2$	→	$[Mo](N_2) + NH_3$	−87.98	**−132.35** (−49.90)	**−44.37** (+38.08)	−86.78	−43.79	+42.99
$[Mo](NH_3)$	→	$[Mo] + NH_3$	+95.77	**+7.45** (+89.90)	**−88.32** (−5.87)	+87.52	+87.15	−0.37
$[Mo] + N_2$	→	$[Mo](N_2)$	−183.75	−139.80	+43.95	−174.29	−130.93	+43.36

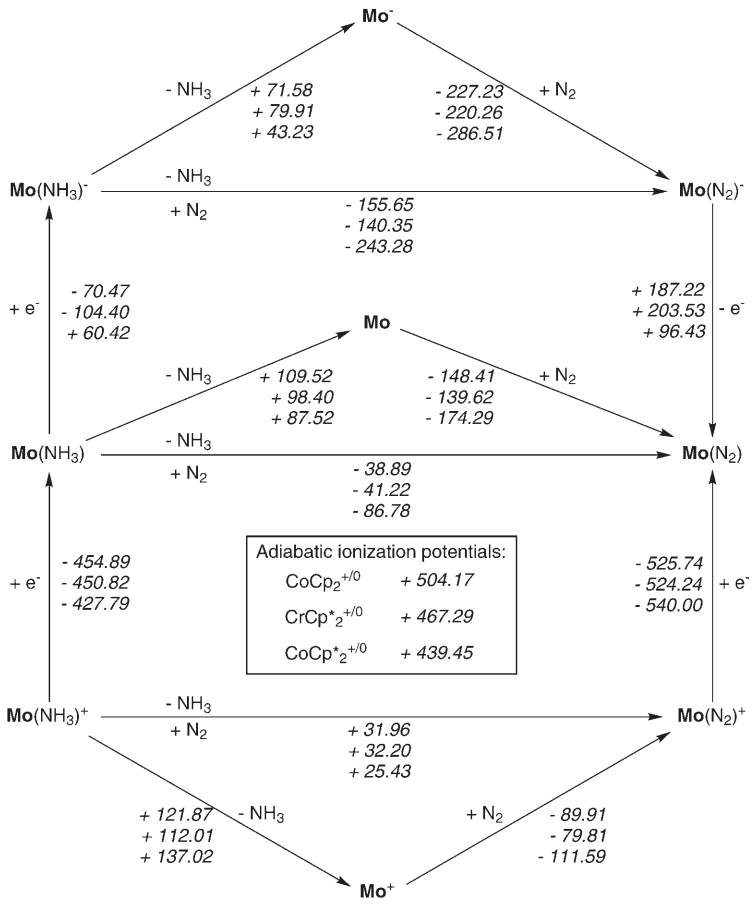

Figure 5. Possible reaction steps (with enegies in kJ mol^{-1}) for the NH$_3$/N$_2$ ligand exchange reaction for system **3** (upper values), model **A** (middle values) and model **B** (lower values). All energies are calculated from the total electronic energies of products minus the ones for the reactants according to the reaction arrows. Accordingly, the adiabatic ionization potentials have been calculated from fully optimized structures (BP86/RI/TZVP) for the reaction metallocene → metallocene$^+ + e^-$.

The last step to complete Schrock's catalytic dinitrogen reduction cycle will be the transfer of a proton onto a [Mo](NH$_2$) species. The product is the $[Mo](NH_3)^+$ complex, which is the first species of relevance to the subsequent exchange of ammonia versus dinitrogen. In principle, exchange of ligands is possible in the cationic state, but the ionization energy indicates that reduction to the neutral species is highly exothermic [Eq. (2)], that is, the ionization energy IE_{NH_3} is endothermic by more than +427 kJ mol^{-1} (compare Figure 5).

$$[Mo](NH_3) \rightarrow [Mo](NH_3)^+ + e^- \quad IE_{NH_3} \qquad (2)$$

On the other hand, the reduction of the N$_2$ cationic complex is even more exothermic and the corresponding ionization energy IE_{N_2} for the reverse reaction [Eq. (3)] is about +525 kJ mol^{-1} for the large systems and +540 kJ mol^{-1} for the small model **B**.

$$[Mo](N_2) \rightarrow [Mo](N_2)^+ + e^- \quad IE_{N_2} \qquad (3)$$

We note that in both cases, complex **3** and model **A** yield almost equivalent results, indicating that the steric effects of the substituted chelate ligand of **3** do not play a significant role.

Coming back to the experimental observations mentioned already in the previous section, we find the experimental result that $[Mo](NH_3)^+$ is more difficult to reduce than $[Mo](N_2)^+$ [13] is supported by our calculations. The authors of reference [13] further assumed that "this substantial difference can be ascribed to the stronger σ-donating properties of ammonia, as well as the fact that the electron added to $[Mo](N_2)^+$ can go into π-bonding orbitals

that are largely located on dinitrogen". This assumption is corroborated by our analysis so far (cf. the previous section).

In contrast to the ionization energies of the different triamidoamine complexes, the electron affinities of the neutral species largely differ for **3**, **A**, and **B**. Reduction of the neutral ammine complexes [Eq. (4)] is exothermic for the large complex **3** and model **A**, but endothermic for models **B** and **C** (compare Figure 5 and Table 4).

$$[\mathrm{Mo}](\mathrm{NH_3}) + \mathrm{e}^- \rightarrow [\mathrm{Mo}](\mathrm{NH_3})^- \qquad \mathrm{EA_{NH_3}} \tag{4}$$

Also, the deviation of the electron affinity calculated for model **A** from the less exothermic electron affinity obtained for **3** is 26 kJ mol^{-1}. The situation is similar for the electron affinities EA_{N_2} of the [Mo](N_2) reduction reaction [Eq. (5)], the exothermicity of which increases in the order: model **B** ($EA_{N_2} = -96.43$ kJ mol^{-1}), complex **3** ($EA_{N_2} = -187.22$ kJ mol^{-1}), and model **A** ($EA_{N_2} = -203.53$ kJ mol^{-1}).

$$[\mathrm{Mo}](\mathrm{N_2}) + \mathrm{e}^- \rightarrow [\mathrm{Mo}](\mathrm{N_2})^- \qquad \mathrm{EA_{N_2}} \tag{5}$$

Evidently, the chelate ligand is able to tune this electron affinity. Since the metallocene reductants deployed in experiment possess ionization potentials too large to reduce the ammine complexes (see the inlay in Figure 5 for calculated values), the reduction of [Mo](NH_3) may only be achieved by other N_xH_y coordinated triamidoamine species present in solution with ionization potentials comparable in absolute value to EA_{NH_3}.

In general, we expect that solvent effects play only a minor role for the dinitrogen reduction cycle at the molybdenum central ion, since the experimentally known systems show a small cavity hardly accessible by large solvent molecules like heptane. However, for the reliable calculation of electron-transfer reactions the solvent environment would have to be taken into account in order to avoid the artificially large ionization energies and electron affinities and to compensate the excess charge. This is a method-inherent problem in the computational chemistry of reduction and protonation processes for isolated molecules as differential solvent effects cannot be taken into account properly if one does not want to use explicit solvation in a molecular dynamics framework. The effect of the environment in compensating the work for charge separation or recombination for the isolated complexes might be estimated by some flavor of electrostatic polarizable continuum models,[69] which would, however, introduce additional parameters affecting the computed results.

Therefore, we calculate the *intrinsic* ionization energies and electron affinities for the isolated system, which may be compared with those of the *isolated* reductant and acid. However, an explicit comparison of this kind, especially if only the relative energies to a selected reductant are given, would give the impression of definite reaction energies though they are actually given only with respect to a certain model of the reducing and pronating reagents. In experiment,[8,12,13] three different metallocenes, $CoCp_2$, $CoCp_2$*, and $CrCp_2$* (Cp = cyclopantadiene, Cp* = pentamethylcyclopentadiene), have been tested. The gas-phase ionization potentials of the isolated molecules have been calculated and included in Figure 5. From the BP86/RI/TZVP calculation of the ionization process of these metallocenes, we note that reduction of [Mo]$(NH_3)^+$ to [Mo](NH_3) with $CoCp_2$* would be exothermic, while the reduction with $CrCp_2$* is almost thermoneutral and with $CoCp_2$ it is hardly possible. The deprotonation energy of the acid used in experiment is calculated to be 1000.2 kJ mol^{-1} for 2,6-LuH$^+$/2,6-Lu (2,6-Lu = {2,6-lutidinium}{BAr′$_4$}).

Reaction energetics: Before we come to the general discussion of coordination energies, we should have a look on the B3LYP coordination energies and compare with the BP86/RI results in Table 4. As in the case of the electron affinities large discrepancies between the BP86/RI and the B3LYP energies are observed for the ammine complex of model **C**. For the coordination of dinitrogen to the metal fragment [Mo] of models **B** and **C**, we observe an energy deviation of about 44 kJ mol^{-1} between BP86/RI and B3LYP for both models. Hence, the coordination energy is by 44 kJ mol^{-1} less exothermic in the B3LYP calculations but this deviation is consistent for both models. Accordingly, the ligand exchange reactions in Table 4 exhibit deviations from +28.51 to +42.99 kJ mol^{-1}, which can be traced back to the same reasons found for the deviation of BP86/RI and B3LYP in case of N_2 coordination to the metal fragment. Thus, the reason for these deviations may be either an inaccurate quantum chemical treatment of the isolated N_2 ligand or of the N_2 metal complexes. From reference [70] (compare reaction A.I in this reference) we understand that the difference between BP86 and B3LYP reaction energies of the isolated dinitrogen molecule are of the order of 15 kJ mol^{-1} and may attribute the remaining difference to the neutral dinitrogen complex. By contrast, the ammine complex of model **B** is calculated with almost the same accuracy using the BP86/RI or the B3LYP functional (the deviation is only −0.37 kJ mol^{-1}). From this comparison we may conclude for the coordination energies to be discussed in the following that coordination of dinitrogen may be affected by a maximum error of about 40 kJ mol^{-1} if we regard the absolute maximum difference of BP86/RI and B3LYP results as a measure for the reliability of present day DFT methods.

Please note that all energetics have been obtained for low-spin species. Studt and Tuczek[65] found, however, that high-spin states may become important. We can confirm that the cationic ammine complex [Mo]$(NH_3)^+$ indeed possesses a triplet ground state independent of the density functional. For model **B** we found this triplet state by −38.4 kJ mol^{-1} with BP86, by −45.2 kJ mol^{-1} with B3LYP* from references [27,29,30], and by −51.0 kJ mol^{-1} with B3LYP more stable than the lowest lying singlet state. The differences of these splittings are small compared to the accuracy of DFT results in general and follow the trend described in references [27,29,30]. In the following sections, however, we present

all energies for the low-spin potential-energy surfaces, which are either of singlet- or doublet-spin character.

Dissociation of ammonia: For the ammonia versus dinitrogen exchange it is essential to understand the coordination energetics of ammonia to the triamidoamine–metal fragments in different charged states. Ammonia dissociation is endothermic as expected, but requires the less energy the more electrons are transferred onto the molybdenum metal fragment. That is, ammonia abstraction is most easily possible from the monoanionic complex (for complex **3**, 71.58 kJ mol^{-1} are required) and should be feasible at ambient temperatures. Dissociation might also be possible from the neutral species at higher temperatures, which requires up to about 100 kJ mol^{-1} and is thus by about 20 to 30 kJ mol^{-1} larger than for the anionic complex. The cationic complex [Mo](NH$_3$)$^+$ requires an energy of 112.01 to 137.02 kJ mol^{-1} depending on the chelate ligand derivative. An additional amount of up to 50 kJ mol^{-1} is required for ammonia abstraction when compared with the neutral species. However, no trend is observed with respect to the increasing complexity of the ligand in system **B** to **A** to **3**. Complex **3** shows the smallest difference in dissociation energy for [Mo](NH$_3$) (+109.52 kJ mol^{-1}) and [Mo](NH$_3$)$^+$ (+121.87 kJ mol^{-1}). Hence, dissociation of ammonia from the neutral and cationic species of complex **3** is almost equally feasible. We emphasize that the dissociation energetics from the various charged ammine complexes of the smallest model series **B** show the most pronounced differences when dissociating ammonia from the anionic (+43.24 kJ mol^{-1}), the neutral (+87.52 kJ mol^{-1}), or the cationic (+137.47 kJ mol^{-1}) ammine complex.

Coordination of dinitrogen: The coordination of dinitrogen is exothermic in all cases. The exothermicity of the coordination reaction depends largely on the charge of the metal fragment. In the case of the monoanion, the reaction is by more than −220 kJ mol^{-1} exothermic, which is very remarkable. The neutral metal fragments bind N_2 still by about −140 kJ mol^{-1} or more depending on the chelate ligand. The gain of energy by coordination of dinitrogen to the cationic complex fragment yields at most about −110 kJ mol^{-1}. This trend of decreased coordination energies is in accordance with the population of the stabilized frontier molecular orbital 47a in Figure 3 as discussed above.

The *trans*-effect of the amine nitrogen atom of the chelate ligands may also play a role in modulating the coordination energy of N_2 as demonstrated in reference [71]. The rigidity of the chelate ligand limits the spatial relaxation of the amine nitrogen atom in the chelate ligand in *trans*-position so that the calculated coordination energy may be regarded as an upper limit for N_2 coordination. However, a test calculation on an oversimplified dinitrogen-coordinating model [Mo(NH$_3$)(NH$_2$)$_3$(N$_2$)] with a non-clamped ammonia in *trans*-position and three free NH_2^- amide ligands in equatorial position yields a H$_3$N–Mo distance of about 2.23 Å, which is in the range of bond lengths reported in Table 1. However, this structure has not been fully optimized, since one of the three amide ligands would rotate and is then in orthogonal orientation with respect to the remaining two amide ligands.

The NH$_3$-dissociation/N$_2$-coordination step: Since dissociation of NH_3 is facilitated, the more negatively charged the metal complexes are and dinitrogen binding is energetically favored for negatively charged complexes, it is evident that exchange of NH_3 by N_2 at the anionic triamidoamine–metal fragments is exothermic by at least −140.35 kJ mol^{-1}, while it is still energetically favorable for the neutral species (by at least −41.22 kJ mol^{-1}), but endothermic for the cationic species (by +25.88 kJ mol^{-1} or more; see Figure 5 for all ligand exchange energies). Experimental evidence[13] indicates that conversion of the cationic ammine to the cationic dinitrogen complex of species **1** should be slower by at least one order of magnitude than the conversion of the neutral species. Based on this observation, Yandulov and Schrock[13] consider the reduction of the cationic ammine complex to the neutral species as an imperative step for efficient formation of the dinitrogen complex, which is fully corroborated by our quantum chemical results.

From the overall energetics of all possible NH_3/N_2 exchange pathways we conclude that a direct substitution would only be likely to take place if the reaction cavity, the size of which is governed by the chelate ligand, is sufficiently large to accomodate both ligands at the same time. This, however, does not appear to be the case for complex **3**. The chelate ligand of complex **3** is sterically very demanding and leaves only a single entrance channel for N_2 from one side—all other sides are blocked. This unique channel is depicted in Figure 6. Of course, thermal movement of the phenyl substituents may open a new entrance channel for N_2 (depending on the substituents in the [TerN$_3$N]$^{3-}$ ligand), but this would close the channel which was open before for steric reasons. Most important is that the channel is rather narrow and it is unlikely that N_2 approaching from this side will be able to substitute the NH_3 ligand. It should be emphasized that one must not draw conclusion on the size of the cavity on the basis of models **A** and **B**, since these models are oversimplified in this respect.

Thus, an elimination and subsequent addition process appears to be the most probable reaction mechanism for coordination of N_2. The only thermodynamically viable elimination–association pathway appears to be the abstraction of ammonia from the anionic metal fragment, which thus requires a reduction step first. It is also interesting to note that the exchange of ligands is endothermic (or at best thermoneutral if environment and finite temperature effects are taken into account) for the *cationic* complex.

Schrock and co-workers[12] concluded for the conversion step of [Mo](NH$_3$)$^+$ to [Mo](N$_2$) that two key steps are involved: 1) reduction of [Mo](NH$_3$)$^+$ to [Mo](NH$_3$) and 2) replacement of ammonia by dinitrogen. Step 2 is believed to take place through the formation of the bare [Mo] metal fragment though this species has not been observed so far.

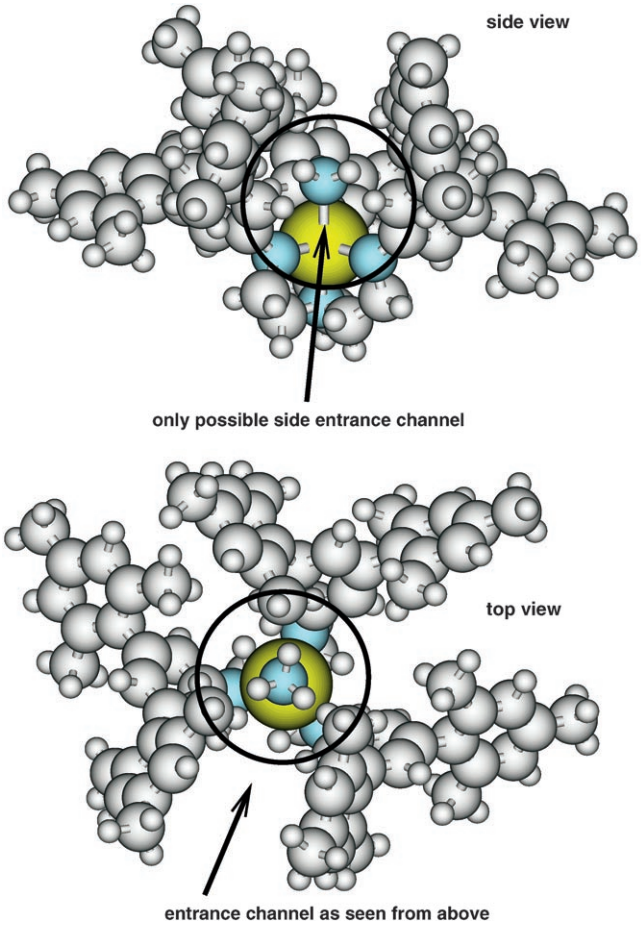

Figure 6. A side and top view of the ammine complex **3**. The side view shows the single channel available for dinitrogen approaching the reaction center to substitute the ammine ligand.

The scheme of potential reactions depicted in Figure 5 offers two possible reaction pathways depending on the reaction conditions. Experimental results for complex **1** clearly show that the cationic ammine complex $[Mo](NH_3)^+$ is an intermediate that is produced in significant amount.[13] If the neutral ammine complex of **3** is reduced to the $[Mo](NH_3)^-$ ion, which is exothermic by $-70.47\,kJ\,mol^{-1}$ provided that an electron can be delivered from a reductant with corresponding ionization energy, NH_3 will dissociate and yield $[Mo]^-$. In a subsequent step, N_2 will coordinate and yield $[Mo](N_2)^-$, which can then be further reduced. The resulting reaction mechanism is given in Equation (6).

$$[Mo](NH_3)^+ \xrightarrow{+e^-} [Mo](NH_3) \xrightarrow{+e^-} [Mo](NH_3)^- \xrightarrow[-NH_3]{} [Mo]^- \xrightarrow{+N_2} [Mo](N_2)^- \xrightarrow{+H^+} [Mo](N_2H) \quad (6)$$

At higher temperatures and without presence of a (very) strong reductant, an alternative route would be the dissociation of NH_3 from the neutral complex to form the metal fragment [Mo]. This neutral metal fragment then coordinates N_2 and needs to be reduced—it is exothermic by $-187.22\,kJ\,mol^{-1}$ for complex **3**—in order to facilitate the first transfer of a proton on the activated anionic N_2 complex. The mechanism then changes to that given in Equation (7).

$$[Mo](NH_3)^+ \xrightarrow{+e^-} [Mo](NH_3) \xrightarrow[-NH_3]{} [Mo] \xrightarrow{+N_2} [Mo](N_2) \xrightarrow{+e^-} [Mo](N_2)^- \xrightarrow{+H^+} [Mo](N_2H) \quad (7)$$

Moreover, since the abstraction of an electron requires a significant amount of energy it is likely that the anionic dinitrogen complex is then protonated. The neutral dinitrogen complex appears to be no imperative intermediate of dinitrogen reduction. However, the concentration of neutral dinitrogen complexes will strongly depend on the chelate ligand, since the ionization energy of the anion (equivalent to the electron affinity of the neutral complex) largely depends on the chelate ligand (cf. Figure 5). Accordingly, the effect of different derivatives of the chelate ligand is not solely a kinetic one owing to varying steric effects, but exerts thermodynamic effects.

Cao and co-workers[22] studied a simplified model with a $[(PhN)_3N]^{3-}$ ligand using the BLYP and PW91 density functionals. Their results are in accordance with our findings for models **A** and **B** and thus supplement the series of model systems investigated here. A close comparison with the work of Cao et al. is, however, hardly possible as these authors have considered only the second route of the two possible mechanisms, for which they gave not many details.

The fact that reduction of the ammonia complex or metal fragment facilitates dinitrogen binding is known from experimental facts for molybdenum complexes and Schrock et al. note:[13] "[..] conversion of $[Mo](NH_3)^+$ into $[Mo](N_2)^+$ would appear to be slower by at least an order of magnitude than the conversion of $[Mo](NH_3)$ into $[Mo](N_2)$ … Conversion of $[Mo](NH_3)^+$ into $[Mo](NH_3)$ facilitates the exchange of ammonia for dinitrogen, which is what one would conclude simply upon considering bonding of ammonia versus dinitrogen to a positively charged Mo^{IV} center versus a neutral Mo^{III} center. Therefore, reduction of $[Mo](NH_3)^+$ to $[Mo](NH_3)$ would appear to be imperative for efficient formation of $[Mo](N_2)$."

From Davidson–Roby–Ahlrichs partial charges reported in Table 5 we understand that the molybdenum atom is positively charged in all ammine and dinitrogen complexes, irrespective of the charge of the complex and of the chelate ligand. However, the trend from cationic to anionic species clearly shows a reduction of this positive partial charge on the molybdenum atom. Interestingly, the partial charge on the nitrogen atom of N_2 coordinated to the central metal ion is also positive and increased in this order. By contrast, the *negative* partial charge of the nitrogen atom in the NH_3 ligand of complex **3** is decreased in the order from cationic to neutral to anionic. The ammine complexes of the models **A** and **B**, however, do not show clear trends (compare the second set of three rows of blocks two and three in Table 5). Taking the amide and amine nitrogen atoms of the chelate ligand sphere into account the results given in Table 5 also

Table 5. Davidson–Roby–Ahlrichs population analysis with multicenter corrections for the analysis of partial charges (notation is according to Figure 2).

	Mo	N_{ad}	N_{am}	N_{α}	N_{β}
complex **3**					
$[Mo](N_2)^-$	0.433	−0.272	−0.063	0.232	−0.359
$[Mo](N_2)$	0.539	−0.366	−0.055	0.168	−0.149
$[Mo](N_2)^+$	0.565	−0.286	−0.035	0.104	−0.013
$[Mo](NH_3)^-$	0.386	−0.304	0.083	−0.084	
$[Mo](NH_3)$	0.630	−0.331	0.052	−0.104	
$[Mo](NH_3)^+$	0.602	−0.289	0.047	−0.123	
model **A**					
$[Mo](N_2)^-$	0.862	0.056	0.064	0.474	−0.184
$[Mo](N_2)$	0.886	0.213	0.095	0.367	0.007
$[Mo](N_2)^+$	1.092	0.349	0.193	0.366	0.185
$[Mo](NH_3)^-$	0.784	0.143	0.222	0.037	
$[Mo](NH_3)$	0.819	0.193	0.203	−0.026	
$[Mo](NH_3)^+$	0.941	0.259	0.209	−0.010	
model **B**					
$[Mo](N_2)^-$	0.382	−0.369	−0.045	0.228	−0.422
$[Mo](N_2)$	0.561	−0.338	−0.029	0.145	−0.163
$[Mo](N_2)^+$	0.591	−0.249	−0.027	0.091	0.039
$[Mo](NH_3)^-$	0.441	−0.324	0.245	−0.200	
$[Mo](NH_3)$	0.569	−0.365	0.084	−0.195	
$[Mo](NH_3)^+$	0.579	−0.239	0.049	−0.223	

do not exhibit any evident trends. The two electrons added to the cationic and neutral states to give the anion are thus distributed on the whole complex.

Conclusions

This work represents a first part of a series of DFT studies on Schrock-type triamidoamine–molybdenum complexes to understand dinitrogen reduction under mild ambient conditions from a quantum chemical point of view. The study provides thermochemical data for all intermediates involved in the first ammonia-dissociation/dinitrogen-binding step.

On the basis of our results obtained for complex **3** and model **A**, we draw the general conclusions that two routes of the mechanism are feasible for the ligand exchange step in the Schrock cycle. In the presence of a strong reductant, the following elementary steps [Eq. (8)] are likely to take place:

$$[Mo](NH_3) \xrightarrow{+e^-} [Mo](NH_3)^- \xrightarrow[-NH_3]{} [Mo]^- \xrightarrow{+N_2} [Mo](N_2)^- \qquad (8)$$

If, however, reduction of the neutral ammine complex cannot be achieved, an alternative route [eventually at higher tenperatures; Eq. (9)] will be the pathway.

$$[Mo](NH_3) \xrightarrow[-NH_3]{} [Mo] \xrightarrow{+N_2} [Mo](N_2) \xrightarrow{+e^-} [Mo](N_2)^- \qquad (9)$$

Both pathways appear to be consistent with experimental findings that different routes for the catalytic cycle are possible.[13]

The different chelate ligand derivatives exert pronounced electronic effects on reaction energies. Models **B** and **C** turned out to be rather inadequate model complexes when it comes to a quantitative understanding of the catalytic action of the triamidoamine complex. Especially for the coordination reactions of N_2 and NH_3, we found large deviations of the small model complexes **B** and **C** from the results obtained for the larger model **A** and the experimentally known complex **3**. The effect is less pronounced if the dissociation–addition reaction is calculated directly, since the effects for ammonia dissociation and dinitrogen coordination cancel. Only model **A**, which is the generic ligand for the $[TerN_3N]^{3-}$ class of ligands, shows good agreement with complex **3**. While the general qualitative picture will be valid also for all model systems, it is even qualitatively different for the reduction of the ammine complex to the anionic species $[Mo](NH_3)^-$. However, in this case even the largest model **A** does not show quantitative agreement with the energies calculated for complex **3**. These results indicate that the true energetics of Schrock's triamidoamine complexes should be assessed from the full systems.

A technical side note on computational studies appears to be appropriate at this place: We observe a surprisingly small variation in coordination energies for N_2 and NH_3 calculated with BP86 and B3LYP density functionals from structures optimized with the corresponding functionals. These differences shed light on the overall reliability of calculated reaction energies within the DFT framework. Pure and hybrid density functionals yield, in general, consistent structural parameters and consistent energetics for triamidoamine–molybdenum complexes.

The next two parts of this series of papers will consider 1) the thermochemistry of the transfer of protons on the coordinated nitrogen ligands and 2) a detailed comparison of the experimentally most well-known and most efficient triamidoamine derivative **1** with results from DFT calculations.

Acknowledgments

Financial support by the collaborative research centers SFB 436 ("Metallvermittelte Reaktionen nach dem Vorbild der Natur", Jena) and SFB 624 ("Template", Bonn) as well as by the Fonds der Chemischen Industrie (FCI) are gratefully acknowledged. M.R. thanks the FCI for a Dozentenstipendium.

[1] J. Chatt, J. R. Dilworth, R. L. Richards, *Chem. Rev.* **1978**, *78*, 589–625.
[2] M. Hidai, Y. Mizobe, *Chem. Rev.* **1995**, *95*, 1115–1133.
[3] D. Sellmann, J. Sutter, *Acc. Chem. Res.* **1997**, *30*, 460–469.
[4] M. D. Fryzuk, S. A. Johnson, *Coord. Chem. Rev.* **2000**, *200–202*, 379–409.
[5] *Nitrogen Fixation at the Millenium* (Ed.: G. J. Leigh), Elsevier, Amsterdam, **2002**.
[6] O. Einsle, F. A. Tezcan, S. L. A. Andrade, B. Schmid, M. Yoshida, J. B. Howard, D. C. Rees, *Science* **2002**, *297*, 1696–1700.
[7] B. A. MacKay, M. D. Fryzuk, *Chem. Rev.* **2004**, *104*, 385–401.
[8] D. V. Yandulov, R. R. Schrock, *Science* **2003**, *301*, 76–78.
[9] R. R. Schrock, *Chem. Commun.* **2003**, 2389–2391.

[10] D. V. Yandulov, R. R. Schrock, *J. Am. Chem. Soc.* **2002**, *124*, 6252–6253.
[11] D. V. Yandulov, R. R. Schrock, A. L. Rheingold, C. Ceccarelli, W. Davis, *Inorg. Chem.* **2003**, *42*, 796–813.
[12] V. Ritleng, D. V. Yandulov, W. W. Weare, R. R. Schrock, A. S. Hock, W. M. Davis, *J. Am. Chem. Soc.* **2004**, *126*, 6150–6163.
[13] D. V. Yandulov, R. R. Schrock, *Inorg. Chem.* **2005**, *44*, 1103–1117.
[14] B. Hinnemann, J. K. Nørskov, *J. Am. Chem. Soc.* **2003**, *125*, 1466–1467.
[15] J. Schimpl, H. M. Petrilli, P. E. Blöchl, *J. Am. Chem. Soc.* **2003**, *125*, 15772–15778.
[16] T. Lovell, T. Liu, D. A. Case, L. Noodleman, *J. Am. Chem. Soc.* **2003**, *125*, 8377–8383.
[17] I. Dance, *Chem. Commun.* **2003**, 324–325.
[18] V. Vrajmasu, E. Münch, E. L. Bominaar, *Inorg. Chem.* **2003**, *42*, 5974–5988.
[19] U. Huniar, R. Ahlrichs, D. Coucouvanis, *J. Am. Chem. Soc.* **2004**, *126*, 2588–2601.
[20] B. Hinnemann, J. K. Nørskov, *J. Am. Chem. Soc.* **2004**, *126*, 3920–3927.
[21] J. Kästner, P. E. Blöchl, *Inorg. Chem.* **2005**, *44*, 4568–4575.
[22] Z. Cao, Z. Zhou, H. Wan, Q. Zhang, *Int. J. Quantum Chem.* **2005**, *103*, 344–353.
[23] J. P. Perdew, K. Burke, M. Ernzerhof, *Phys. Rev. Lett.* **1996**, *77*, 3865–3868.
[24] B. Hammer, L. B. Hansen, J. K. Nørskov, *Phys. Rev. B* **1999**, *59*, 7413–7421.
[25] A. D. Becke, *Phys. Rev. A* **1988**, *38*, 3098–3100.
[26] J. P. Perdew, *Phys. Rev. B* **1986**, *33*, 8822–8824.
[27] M. Reiher, O. Salomon, B. A. Hess, *Theor. Chem. Acc.* **2001**, *107*, 48–55.
[28] H. Paulsen, L. Duelund, H. Winkler, H. Toftlund, A. X. Trautwein, *Inorg. Chem.* **2001**, *40*, 2201–2203.
[29] M. Reiher, *Inorg. Chem.* **2002**, *41*, 6928–6935.
[30] O. Salomon, M. Reiher, B. A. Hess, *J. Chem. Phys.* **2002**, *117*, 4729–4737.
[31] R. Poli, J. N. Harvey, *Chem. Soc. Rev.* **2003**, *32*, 1–8.
[32] J. N. Harvey, M. Aschi, *Faraday Discuss.* **2003**, *124*, 129–143.
[33] A. Fouqueau, S. Mer, M. E. Casida, L. M. Lawson Daku, A. Hauser, T. Mineva, F. Neese, *J. Chem. Phys.* **2004**, *120*, 9473.
[34] A. Fouqueau, M. E. Casida, L. M. Lawson Daku, A. Hauser, F. Neese, *J. Chem. Phys.* **2005**, *122*, 044110.
[35] G. Ganzenmüller, N. Berkaine, A. Fouqueau, M. E. Casida, M. Reiher, *J. Chem. Phys.* **2005**, *122*, 234321.
[36] L. M. Lawson Daku, A. Vargas, A. Hauser, A. Fouqueau, M. E. Casida, *ChemPhysChem* **2005**, *6*, 1393–1410.
[37] D. C. Graham, G. J. O. Beran, M. Head-Gordon, G. Christian, R. Stranger, B. F. Yates, *J. Phys. Chem. A* **2005**, *109*, 6762–6772.
[38] K. D. Demadis, S. M. Malinak, D. Coucouvanis, *Inorg. Chem.* **1996**, *35*, 4038–4046.
[39] Y. Nishibayashi, I. Wakiji, K. Hirata, M. Rakowski Du Bois, M. Hidai, *Inorg. Chem.* **2001**, *40*, 578–580.
[40] R. K. Szilagyi, D. G. Musaev, K. Morokuma, *Inorg. Chem.* **2001**, *40*, 766–775.
[41] N. L. Grand, K. W. Muir, F. Y. Pétillon, C. J. Pickett, P. Schollhammer, J. Talarmin, *Chem. Eur. J.* **2002**, *8*, 3115–3127.
[42] F. Barriere, *Coord. Chem. Rev.* **2003**, *236*, 71–89.
[43] J. Bell, A. J. Dunford, E. Hollis, R. A. Henderson, *Angew. Chem.* **2003**, *115*, 1181–1184; *Angew. Chem. Int. Ed.* **2003**, *42*, 1149–1152.
[44] L. C. Seefeldt, I. G. Dance, D. R. Dean, *Biochemistry* **2004**, *43*, 1401–1409.
[45] J. K. P. Metzker, J. E. McGrady, *Chem. Eur. J.* **2004**, *10*, 6447–6455.
[46] K. Mersmann, K. H. Horn, N. Böres, N. Lehnert, F. Studt, F. Paulat, G. Peters, I. Ivanovic-Burmazovic, R. van Eldik, F. Tuczek, *Inorg. Chem.* **2005**, *44*, 3031–3045.
[47] R. Ahlrichs, M. Bär, M. Häser, H. Horn, C. Kölmel, *Chem. Phys. Lett.* **1989**, *162*, 165–169.
[48] A. D. Becke, *J. Chem. Phys.* **1993**, *98*, 5648–5652.
[49] P. J. Stephens, F. J. Devlin, C. F. Chabalowski, M. J. Frisch, *J. Phys. Chem.* **1994**, *98*, 11623–11627.
[50] K. Eichkorn, O. Treutler, H. Öhm, M. Häser, R. Ahlrichs, *Chem. Phys. Lett.* **1995**, *240*, 283–290.
[51] K. Eichkorn, F. Weigend, O. Treutler, R. Ahlrichs, *Theor. Chem. Acc.* **1997**, *97*, 119–124.
[52] A. Schäfer, C. Huber, R. Ahlrichs, *J. Chem. Phys.* **1994**, *100*, 5829–5835.
[53] A. Schäfer, H. Horn, R. Ahlrichs, *J. Chem. Phys.* **1992**, *97*, 2571–2577.
[54] D. Andrae, U. Häussermann, M. Dolg, H. Stoll, H. Preuß, *Theor. Chim. Acta* **1990**, *77*, 123–141.
[55] E. R. Davidson, *J. Chem. Phys.* **1967**, *46*, 3320–3324.
[56] K. R. Roby, *Mol. Phys.* **1974**, *27*, 81–104.
[57] R. Heinzmann, R. Ahlrichs, *Theor. Chim. Acta* **1976**, *42*, 33–45.
[58] W. Koch, M. C. Holthausen, *A Chemist's Guide to Density Functional Theory*, Wiley-VCH, Weinheim, **2000**.
[59] M. Reiher, O. Salomon, D. Sellmann, B. A. Hess, *Chem. Eur. J.* **2001**, *7*, 5195–5202.
[60] M. Reiher, B. A. Hess, *Chem. Eur. J.* **2002**, *8*, 5332–5339.
[61] M. Reiher, J. Neugebauer, B. A. Hess, *Z. Phys. Chem.* **2003**, *217*, 91–103.
[62] J. N. Harvey, *Struct. Bonding* **2004**, *112*, 151–183.
[63] R. Hoffmann, *J. Chem. Phys.* **1963**, *39*, 1397–1412.
[64] C. Mealli, D. M. Proserpio, *J. Chem. Educ.* **1990**, *67*, 399–402.
[65] F. Studt, F. Tuczek, *Angew. Chem.* **2005**, *117*, 5783–5787; *Angew. Chem. Int. Ed.* **2005**, *44*, 5639–5642. .
[66] *NIST Chemistry WebBook*, *NIST Standard Reference Database Number 69* (Eds.: P. J. Linstrom, W. G. Mallard), National Institute of Standards and Technology, Gaithersburg MD, 20899 (http://webbook.nist.gov), June **2005**.
[67] M. Reiher, B. Kirchner, J. Hutter, D. Sellmann, B. A. Hess, *Chem. Eur. J.* **2004**, *10*, 4443–4453.
[68] B. Kirchner, M. Reiher, A. Hille, J. Hutter, B. A. Hess, *Chem. Eur. J.* **2005**, *11*, 574–583.
[69] J. Tomasi, B. Mennucci, R. Cammi, *Chem. Rev.* **2005**, *105*, 2999–3094.
[70] M. Reiher, J. Neugebauer, B. A. Hess, *Z. Phys. Chem.* **2003**, *217*, 91–103.
[71] G. Moritz, M. Reiher, B. A. Hess, *Theor. Chem. Acc.* **2005**, 114, 76–83.

Received: August 2, 2005
Published online: November 3, 2005

